

1 **Comprehensive modelling study on observed new particle**
2 **formation at the SORPES station in Nanjing, China**

3
4 **X. Huang^{1,2}, L. X. Zhou^{3,4}, A. J. Ding^{1,2,*}, X. M. Qi^{1,2}, W. Nie^{1,2}, M. H. Wang^{1,2}, X. G.**
5 **Chi^{1,2}, T. Petaja³, V.-M. Kerminen³, P. Roldin³, A. Rusanen³, M. Kulmala³, and M.**
6 **Boy³**

7
8 ¹Institute for Climate and Global Change Research & School of Atmospheric Sciences,
9 Nanjing University, Nanjing, 210023, China

10 ²Collaborative Innovation Center of Climate Change, Nanjing, Jiangsu Province, China

11 ³Department of Physics, University of Helsinki, P. O. Box 64, 00014 University of Helsinki,
12 Finland

13 ⁴Helsinki University Centre for Environment, P. O. Box 65, 00014 University of Helsinki,
14 Finland

15
16 * Correspondence to: Aijun Ding (dingaj@nju.edu.cn)

1 **Abstract**

2 New particle formation (NPF) has been investigated intensively during the last two decades
3 because of its influence on aerosol population and the possible contribution to cloud
4 condensation nuclei. However, intensive measurements and modelling activities on this topic
5 in urban metropolitans in China with frequently high pollution episodes are still very limited.
6 This study provides results from a comprehensive modelling study on the occurrence of new
7 particle formation events in the western part of the Yangtze River Delta region (YRD), China.
8 The comprehensive modelling system, which combines regional chemical transport model
9 WRF-Chem (the Weather Research and Forecasting model coupled with Chemistry) and the
10 sectional box model MALTE-BOX (the model to predict new aerosol formation in the lower
11 troposphere), was shown to be capable of simulating atmospheric nucleation and subsequent
12 growth. Here we present a detailed discussion of three typical NPF days, during which the
13 measured air masses were notably influenced by either anthropogenic activities, biogenic
14 emissions, or mixed ocean and continental sources. Overall, simulated NPF events were
15 generally in good agreement with the corresponding measurements, enabling us to get further
16 insights into NPF processes in the YRD region. Based on the simulations, we conclude that
17 biogenic organic compounds, particularly monoterpenes, play an essential role in the initial
18 condensational growth of newly formed clusters through their low volatile oxidation products.
19 Although some uncertainties remain in this modelling system, this method provides a
20 possibility to better understand particle formation and growth processes.

21

22 **1 Introduction**

23 Ambient aerosols affect human health adversely, degrade visibility, and play an important
24 role in climate change through directly scattering/absorbing solar radiation or indirectly
25 modifying microphysical properties of clouds (Eidels-Dubovoi, 2002; Davidson et al., 2005;
26 Lohmann and Feichter, 2005; Myhre et al., 2013). Atmospheric new particle formation (NPF),
27 characterized by a sharp increase in number concentration of nucleation-mode aerosol, has
28 been observed under a wide variety of circumstances and has been shown as a significant
29 source of atmospheric fine particles (O'Dowd et al., 2002; Kulmala and Kerminen, 2008; Gao
30 et al., 2011; Guo et al., 2012; Guo et al., 2014; Wang et al., 2014). As the newly formed
31 particles and their following growth may lead several-fold increases in aerosol number
32 concentrations, atmospheric NPF could substantially contribute to the global CCN (Cloud

1 condensation nuclei) budget and its subsequent cooling effect (Lihavainen et al., 2003;
2 Merikanto et al., 2009; Yu and Luo, 2009; Wang and Penner, 2009; Kerminen et al., 2012;
3 Makkonen et al., 2012; Scott et al., 2015).

4 NPF has been extensively and intensively studied globally during the last two decades. It is
5 well known that particle formation in the atmosphere is strongly dependent on the abundance
6 of sulphuric acid (Weber et al., 1999; Kulmala et al., 2004b; Sipila et al., 2010). Meanwhile,
7 other compounds in the atmosphere may be responsible for NPF occurrence in different
8 environments. Iodine-containing vapours were identified as the precursors for marine new
9 particle formation (O'Dowd et al., 2002). Observations in Pittsburgh imply that ammonia
10 could considerably enhance the atmospheric particle formation (Q. Zhang et al., 2004). In the
11 boreal forest, oxidation products of monoterpenes together with sulphuric acid were very
12 likely to lead to NPF (Schobesberger et al., 2013) and new findings indicate that organic
13 amines (e.g. dimethylamine) can enhance water-sulphuric acid particle formation rates more
14 than 1000-fold compared to ammonia (Almeida et al., 2013). In addition to direct in-situ
15 observations of NPF events, model simulation has been serving as a useful tool for analysing
16 NPF dynamics since 1990s (Kulmala et al. 1995; Kerminen and Wexler, 1996; Korhonen et
17 al., 1999). In recent years, MALTE model has been successfully utilized in NPF analysis, for
18 instance, reproducing OH radical and gaseous sulphuric acid levels (Petaja et al., 2009),
19 validating various plausible nucleation mechanisms and particle growth (Boy et al., 2007;
20 Wang et al., 2013b), and identifying important factors influencing NPF occurrence (Boy et al.,
21 2006, 2008; Ortega et al., 2012).

22 As one of the most economically invigorating and densely populated countries, China features
23 simultaneous high aerosol loadings and NPF rates (S. Liu et al., 2008; Gao et al., 2011; Guo
24 et al., 2012). Moreover, the condensational growth of nucleation-mode particles has been
25 indicated as a plausible cause of regional haze events (Guo et al., 2014). Since 2000s, several
26 field campaigns as well as long-term measurements have been conducted in several regions
27 such as Beijing, the Pearl River Delta as well as the Yangtze River Delta, showing high
28 occurrence frequencies and formation rates across China (S. Liu et al., 2008; Gao et al., 2009;
29 Yue et al., 2010; Herrmann et al., 2014; Qi et al., 2015; Xiao et al., 2015). However,
30 modelling studies that provide a further insight into the processes of atmospheric aerosol
31 formation, are still very limited in China. Numerical simulations of formation and growth
32 processes usually require detailed and high time-resolving measurements of the relevant

1 compounds, however, hardly can any field campaign or in-situ measurement station in China
2 meet this requirement. The novel combination of a regional chemical transport model and a
3 zero-dimensional box model with detailed aerosol dynamics makes it possible to accomplish
4 NPF studies without direct measurements of all specific chemical species. Here, we present a
5 comprehensive modelling study targeting at reproducing observed NPF events under distinct
6 conditions at the Station for Observing Regional Processes of the Earth System (SORPES) at
7 Nanjing University in Nanjing, China (Ding et al., 2013a). This is the first attempt to integrate
8 the regional model, box model and in-situ measurements to investigate NPF events in China,
9 enabling us to gain more insights into NPF mechanism in the YRD region.

10

11 **2 Data and Methodology**

12 **2.1 In-situ measurements**

13 The SORPES site is located in the Xianlin campus of Nanjing University in the suburban area
14 northeast of Nanjing, which is about 20 km east from the downtown area (118°57'10'' E,
15 32°7'14''N, 40 m a.s.l. as shown in Fig. 1 in Ding et al., 2013a). This site, with few local
16 emission sources around it, is generally upwind of downtown Nanjing and also downwind of
17 the city clusters of the Yangtze River Delta. Hence it can be regarded as a regional
18 background station (Ding et al., 2013a).

19 On-line and high time-resolving measurements of trace gases, aerosol characteristics, and
20 relevant meteorological parameters have been conducted since the summer of 2011. Ozone
21 (O_3), sulphur dioxide (SO_2), nitrogen monoxide (NO), nitrogen dioxide (NO_2), total reactive
22 nitrogen (NO_y), carbon monoxide (CO) and $PM_{2.5}$ (fine particulates less than 2.5 microns in
23 aerodynamic diameter) are routinely measured by Thermo Instruments (TEI 49i, 43i, 42i,
24 42iY and 48i) and MARGA (Monitor for Aerosols & Gases in Ambient Air) (Ding et al.,
25 2013a,b). The Differential Mobility Particle Sizer (DMPS) coupling a differential mobility
26 analyzer with two different flow rates and a condensation particle counter are used to measure
27 number distributions of atmospheric particles from 6 to 800 nm (Herrmann et al., 2014, Qi et
28 al., 2015). More thorough information on the instruments at the SORPES site is elaborated in
29 detail in Ding et al. (2013a,b).

1 2.2 Model description

2 2.2.1 MALTE-BOX model

3 MALTE is a one-dimension model comprising of boundary layer meteorology, biogenic
4 emission of volatile organic compounds, gas-phase chemistry and aerosol dynamics in order
5 to predict particle formation and growth processes under atmospheric conditions (Boy et al.,
6 2006). Here, we apply the zero-dimensional version, namely, MALTE-BOX model, to
7 simulate NPF events at the SORPES station. In the MALTE-BOX model, boundary layer
8 meteorology and biogenic emission modules are switched off; instead, the biogenic and
9 anthropogenic VOC emissions and their following transport and dispersion are calculated by
10 the regional chemical transport model WRF-Chem. Concentration of various organic
11 compounds at the SORPES station predicted by WRF-Chem model are inputted into
12 MALTE-BOX model every 10 minutes (Table 1 provides the compounds calculated by WRF-
13 Chem as input to MALTE-BOX). Likewise, measured concentrations of trace gases including
14 CO, SO₂, NO, NO₂ and O₃, with the same temporal resolution, are also included as input
15 fields. In addition to gas phase precursors, the inputs also include an initial particle number
16 size distribution at 0:00 LT on each day, ambient temperature, relative humidity and the
17 condensation sink of sulphuric acid (as defined in Sect. 2.3).

18 In the MALTE-BOX model, particles are assumed to be spherical. Fixed sectional approach
19 with 40 size bins ranging from 1.4 to 2000 nm in diameter is used in the present study. The
20 aerosol dynamics has all basic aerosol processes, including nucleation, condensation,
21 coagulation, and deposition. The new particle formation rates of newly formed clusters are
22 estimated by the kinetic nucleation theory of sulphuric acid (Sihto et al., 2006), which is
23 related to the sulphuric acid concentration as follows:

$$24 \quad J = k_1 \times [\text{H}_2\text{SO}_4]^2 \quad \text{Eq. 1}$$

25 where k_1 is the kinetic coefficient that includes both the collision frequency and the
26 probability of forming a stable cluster after the collision. Kinetic nucleation theory has been
27 shown to have good performance in simulating cluster formation in various environments
28 including both clean continental area and polluted urban site (Wang et al., 2013b; Zhou et al.,
29 2014). The nucleated particles were added to the first size bin in the model.

30 We conducted a set of sensitivity simulations to establish a suitable value for the nucleation
31 coefficient k_1 . After comparing the simulations and DMPS measurements, k_1 was set to

1 $6.0 \times 10^{-13} \text{ cm}^3/\#$ for 10 July and 22 August, and $2.2 \times 10^{-10} \text{ cm}^3/\#$ for 22 June, respectively.
2 These values were similar than those we commonly used in the simulations for NPF at other
3 stations (Boy et al., 2008a, Paasonen et al., 2010; Zhou et al., 2014). The high value on the 22
4 June might imply that other low volatile vapours - most probably from anthropogenic origin -
5 are involved and play a crucial role in the particle formation process at this urban site.
6 Moreover, being limited by the detectable size of the DMPS (what we can monitor are the
7 particles larger than 6 nm in diameter), means that the observed formation process could be
8 steered by the condensational growth of the smallest clusters to the detection limit.

9 We included relevant chemical reactions of the MCM (Master Chemical Mechanism) in this
10 model, as described in Boy et al (2013). The chemistry scheme included the full MCM
11 chemical paths for the following parent molecules: methane, methanol, formaldehyde, acetone,
12 acetaldehyde, 2-methyl-3-buten-2-ol (MBO), isoprene, alpha-pinene, beta-pinene, limonene
13 and beta-caryophyllene. The Kinetic PreProcessor (KPP) was applied to numerically solve for
14 the concentrations of each individual compound (Damian et al., 2002), except for those
15 species whose concentrations were manually inputted from direct measurements and WRF-
16 Chem model. Apart from sulphuric acid, about twenty low-volatility organic compounds
17 (ELVOCs) and seven selected semi-volatile organic compounds (SVOCs) are regarded as
18 condensing vapours, following the simplified chemical mechanism presented by Ehn et al.
19 (2014). Specifically, seven representative SVOCs (MCM-nomenclature: C719OOH,
20 LIMALOOH, C924OOH, NORLIMOOH, C811OOH, C818OOH and C819OOH) with
21 vapour pressures estimated to range from 10^4 to 10^6 molecules cm^{-3} (using the group
22 contribution method described by Nannoolal et al. (2008)) and recently detected ELVOCs
23 ($\text{C}_{10}\text{O}_{5-12}\text{H}_x$, $\text{C}_{10}\text{NO}_{5-13}\text{H}_x$ and $\text{C}_{20}\text{O}_{8-16}\text{H}_x$) with vapour pressures between 10 and 10^3
24 molecules cm^{-3} are included as condensing vapours in the model.

25 2.2.2 WRF-Chem

26 The WRF-Chem version 3.6 was used here to estimate concentrations of various organic
27 vapours from anthropogenic and biogenic emissions as there was no VOCs measurement at
28 the SORPES site during the study period. WRF-Chem is an online three-dimensional,
29 Eulerian chemical transport model that considers the complex physical and chemical
30 processes, such as emission and deposition of pollutants, advection and diffusion, gaseous and
31 aqueous chemical transformation, aerosol chemistry and dynamics (Grell et al., 2005). It is
32 capable of simulating atmospheric chemistry on a regional scale and has been successfully

1 applied in several of our previous studies (Huang et al., 2014, 2015). In this study, the model
2 domain covered East China and its surrounding area, centring at 32.0°N, 119.0°E with a
3 20×20 km grid resolution, as demonstrated in Fig. 1. There are 24 vertical layers from the
4 ground level to the top pressure of 50 hPa, in which 10 layers are placed under 1 km to better
5 resolve the boundary layer process. The 6 hourly Final operational global analysis (FNL) data
6 with a 1°× 1° spatial resolution produced by the National Centres for Environmental
7 Prediction (NCEP) was used as initial and boundary conditions of meteorological fields. The
8 simulations were conducted for June to August 2013 when NPF events were frequently
9 detected (Qi et al., 2015). During the simulation period, each run covered 60 hours, in which
10 the first 12 hours were just for model spin-up and the last 48-hour results were adopted for
11 following analysis and box modelling. The outputs of compound concentrations from the
12 preceding run were treated as the initial conditions for the next run. Key physical
13 parameterization options for the WRF-Chem modelling are the Noah land surface scheme to
14 describe the land-atmosphere interactions (Ek et al., 2003), the Lin microphysics scheme (Lin
15 et al., 1983) with the Grell cumulus parameterization to reproduce the cloud and precipitation
16 processes (Grell and Devenyi, 2002), the YSU boundary layer scheme (Hong, 2010), and the
17 RRTMG short- and long-wave radiation scheme (Mlawer et al., 1997).

18 Anthropogenic emissions from power plants, residential combustion, industrial processes, on-
19 road mobile sources and agricultural activities were derived from the MEIC database (Multi-
20 resolution Emission Inventory for China, see www.meicmodel.org). Emissions of major
21 pollutants, such as carbon monoxide, sulphur dioxide, nitrogen oxides, ammonia and
22 speciated VOCs are all included in this emission inventory database. MEGAN (Model of
23 Emissions of Gases and Aerosols from Nature, version 2) module embedded in WRF-Chem is
24 used to calculate biogenic emissions online (Guenther et al., 2006). It estimates the net
25 emission rates of isoprene, monoterpene and other biogenic VOCs from terrestrial ecosystems
26 into the above-canopy atmosphere. Gas-phase chemistry is explicitly represented by the
27 model through the SAPRC photochemistry scheme (Carter, 1999), which includes 225 gas-
28 phase reactions among 81 chemical species in the model. We mapped some predicted organic
29 species in WRF-Chem to the MALTE-BOX following the correspondence denoted in Table 1.
30 Regarding the monoterpenes (alpha-pinene, beta-pinene, camphene, myrcene, carene and
31 limonene) used in MALTE-BOX chemistry (details in Boy et al., 2013), the distribution was
32 performed equally because no VOC-measurement were available at the SORPES station.

1 2.3 Data analysis

2 The calculations of particle growth and formation rates are conducted following the
3 procedures outlined by Kulmala et al. (2012). The formation rate is obtained from the
4 following equation:

$$5 \quad J_{dp} = \frac{dN_{dp}}{dt} + CoagS_{dp} \times N_{dp} + \frac{GR}{\Delta dp} \times N_{dp} + S_{losses} \quad \text{Eq. 2}$$

6 where J_{dp} refers to the particle formation rate of diameter dp , the first term on the right side is
7 the time evolution of the particle number concentration with size ranging from dp to $dp+\Delta dp$.
8 The second term derives the coagulation loss by the product of coagulation sink ($CoagS_{dp}$)
9 and the number concentration in the size range $[dp, dp+\Delta dp]$. The third term is the growth out
10 of the considered size range, in which GR means measured growth rate. The last term S_{losses}
11 represents additional losses, which were not considered in this study.

12 The growth rate of particles during the NPF events can be expressed as

$$13 \quad GR_{dp} = \frac{d_{p1} - d_{p2}}{t_1 - t_2} \quad \text{Eq. 3}$$

14 where d_{p1} and d_{p2} are the representative of the diameter of nucleated particles at the times t_1
15 and t_2 , respectively. For calculation, d_{p1} and d_{p2} is then defined as the central size of each bin
16 and t_1 and t_2 are the moments when the concentration of this size bin peaks.

17 The condensation sink determines how rapidly condensable vapour molecules will condense
18 onto pre-existing aerosols. It can be derived by DMPS-measured particle number size
19 distribution according to the following method (Kulmala et al., 2001).

$$20 \quad CS = 4\pi D \sum_{dp'} \beta_{m,dp'} dp' N_{dp'} \quad \text{Eq. 4}$$

21 where D is the diffusion coefficient of the condensing vapour, β_m is a transition-regime
22 correction, dp' is the discrete diameter and $N_{dp'}$ is the particle number concentration in
23 respective size bin.

24

25 3 Results and discussions

26 This chapter is divided into two parts. The first subsection provides discussion of measured
27 particle size distributions on three typical NPF days. Air mass transport pathways and

1 parameters that favour the formation of new particles at the SORPES site will be investigated.
2 The second subsection focuses on the numerical simulation of observed NPF events. A further
3 detailed analysis of particle formation and following growth will be presented.

4 **3.1 Observations and data analysis**

5 Summer marks the season with frequent NPF events at the SORPES site, especially in the
6 year of 2013 (Qi et al., 2015). From June to August 2013, 50 NPF events were detected
7 during the 76-day measurement period when DMPS functioned normally, resulting in the
8 particle formation probability of 66%. Among the observed NPF events, three representative
9 cases were identified according to the retroplumes calculated based on Lagrangian dispersion
10 model HYSPLIT (Hybrid Single Particle Lagrangian Integrated Trajectory Model) following
11 the method developed by Ding et al., (2013c). These selected NPF days are 22 June, 10 July
12 and 22 August 2013, when the site was dominantly influenced by air masses from the YRD
13 region, South China, and mixed ocean and continental areas, respectively (Fig. 2).

14 On 22 June 2013, a clear banana-shaped particle size distribution was captured by the DMPS
15 in the morning (9:00-11:00 LT, Fig. 3). According to the DMPS observations, the number
16 concentration of particles with diameter ranging from 6 to 30 nm reached up to $10,000 \text{ \# cm}^{-3}$
17 around 10:00 LT. The formation rate of 6 nm particles, namely J_6 calculated following Eq. 2,
18 was $7.6 \text{ cm}^{-3} \text{ s}^{-1}$. It was generally comparable to those typically observed elsewhere in China,
19 for instance, $0.97\text{-}10.2 \text{ cm}^{-3} \text{ s}^{-1}$ in Hong Kong ($J_{5.5}$) (Guo et al., 2012). The diurnal variations
20 of measured number size distribution and relevant trace gases are demonstrated in Fig. 3. This
21 NPF event featured a large background particle loading with $\text{PM}_{2.5}$ mass concentration
22 exceeding 50 \mu g m^{-3} because the air mass was lingering over city clusters in the YRD region
23 before approaching the SORPES station, as shown in Fig. 2(a). Dense particle emissions from
24 the rapidly urbanized and industrialized YRD region (Fig. 2(e)) corresponded to a high
25 condensation sink of $4.2 \times 10^{-2} \text{ s}^{-1}$, close to those typically observed in other urban areas in
26 China (Gao et al., 2012; Xiao et al., 2015). For the same reason, influenced by the emissions
27 in the YRD region (Fig. 2(d)), SO_2 concentration was observed to be 20–30 ppb, considerably
28 higher than the normally observed level at the site, which is less than 10 ppb during
29 summertime (Ding et al., 2013a). High-concentration of O_3 and increasing radiation intensity
30 were indicative of active ozone photolysis and production of OH radicals, rapid gas-phase
31 oxidation of SO_2 by OH radical and accumulation of gaseous sulphuric acid are expected,
32 leading to the onset of NPF despite the high level of condensation sink. The subsequent

1 growth was fast, with a GR_{6-30} (growth rate from 6 to 30nm) of 12.6 nm h^{-1} . Accumulating
2 sulphuric acid with increasing ozone concentration might be one contributor. In addition, the
3 presence of aromatic-related oxidation products from residential and industrial combustion in
4 the YRD region could also substantially enhance particle formation and subsequent growth by
5 absorption or heterogeneous reactions (R. Y. Zhang et al., 2004; Y. Liu, et al., 2008).

6 On 10 July when the air masses mostly came from the densely wooded area in South China,
7 NPF showed much lower new particle formation rates than on 22 June, yet a slightly faster
8 particle growth rate (Table 2). Previous investigations have revealed that overall GR is
9 correlated with the rate of terpenes reactions with atmospheric photochemical oxidants,
10 highlighting the importance of biogenic VOCs in the particle growth process (e.g. Boy et al.,
11 2003; Kulmala et al., 2004a). During the QUEST (Quantification of Aerosol Nucleation in the
12 European Boundary Layer) field campaign in Hyytiälä, Finland, recorded particle growth
13 rates during NPF events correlated notably with gas-phase monoterpene concentrations,
14 indicating that the oxidation products from biogenic VOCs may dominate particle growth
15 (Laaksonen et al., 2008; Yli-Juuti et al., 2011). The positive correlation between freshly
16 formed particle growth rates and monoterpenes and their oxidation rates by ozone was also
17 verified in Hong Kong, China (Guo et al., 2012). Fig. 2(f) presents the spatial distribution of
18 monoterpene emission rates during summertime across China calculated by the MEGAN
19 model (Li et al., 2012). It is obvious that monoterpene emission is overwhelmingly intensive
20 in South China, which is covered by large areas of broadleaf forests and shrubs. It is plausible
21 that air masses passed over biogenic VOC-rich regions were saturated with sufficiently low
22 volatile oxidation products, which enhanced the observed particle growth. The simulation
23 results from the WRF-Chem model supported this view. Modelled isoprene and terpenes
24 concentrations were 1.2 and 0.15 ppb at the SORPES site during NPF on 10 July, 150% and
25 50% higher than the corresponding values on 22 June. Besides, lower pre-existing particle
26 loading is another cause of faster growth due to less particle surface area for vapours
27 condensation.

28 Another NPF event, characterized by mixed marine and continental source regions, occurred
29 on 22 August. Because of relatively clean air from the ocean and high wind speed of around 8
30 m s^{-1} , $PM_{2.5}$ and SO_2 concentrations were unusually low, only $11.0 \mu\text{g m}^{-3}$ and 2.8 ppb when
31 NPF event took place. Accordingly, the condensation sink fell down to $1.9 \times 10^{-2} \text{ s}^{-1}$. Existing
32 measurements and analysis concluded that the main obstacle for the initial onset of new

1 particle formation at the SORPES site is condensation sink, since SO₂ concentration is always
2 high and there tends to be enough solar radiation as well (Herrmann et al., 2014). So, even
3 though the SO₂ concentration was pretty low during that day, a fairly small condensation sink
4 could trigger the onset of this NPF event. The nuclei growth rate, GR₆₋₃₀, was estimated to be
5 15.7 nm h⁻¹. On one hand, humid air mass transported from the ocean might have favoured
6 the particle growth due to that high humidity could enhance the uptake and oxidation of SO₂
7 and also facilitate the transformation of gaseous nitric acid to particulate ammonium nitrate
8 (Hildemann et al., 1984; Rattigan et al., 2000). As displayed in Fig. 3, the measured relative
9 humidity (RH) was over 80% when the NPF began. On the other hand, the sampling site was
10 also partly influenced by the air masses from the YRD region (Fig. 2(c)), which means that
11 anthropogenic VOCs and oxidation products with low volatility might also exert a notable
12 impact on particle growth.

13 **3.2 Simulations of NPF events**

14 To shed further light on NPF processes at the SORPES station, comprehensive simulations
15 were performed by combining WRF-Chem regional atmospheric transport model and the
16 MALTE-BOX model. Measurements of meteorological fields, trace gases and aerosol
17 characteristics from the SORPES station are input to the box model. In the meantime, input
18 also includes the concentrations of gaseous organic compounds from the WRF-Chem regional
19 model (see Table 1). The simulations were conducted for the aforementioned three NPF days.

20 **3.2.1 Evaluation of simulations by WRF-Chem model**

21 Meteorological conditions play an important part in transport, diffusion, and chemical
22 reactions in the atmosphere. Simulated hourly 2-m temperature and 10-m wind speed were
23 evaluated using hourly temperature and relative humidity observations at the SORPES station.
24 Statistical analysis of model performance for the three NPF days are listed in Table 3,
25 including mean bias (MB) and root mean square error (RMSE). Generally, the model
26 reproduced the observed 2-m temperature and 10-m wind. As mentioned, modelled VOC
27 concentrations, which are vital for NPF simulation, are included as an input field in the
28 MALTE-BOX model. Although there was no VOC measurement during the summer of 2013,
29 the SORPES site and the Environmental Monitoring Centre of Jiangsu Province (118°47'E,
30 32°4'N) were equipped with GC/MS (gas chromatography/mass spectrometry) in the summer
31 of 2014. In order to evaluate model's performance in simulating VOC concentrations, we

1 conducted another WRF-Chem run for the August of 2014 and then compared the model
2 results with corresponding observations. The comparison of alkene, aromatic and isoprene
3 concentrations in Fig. 4(a-c) illustrates that WRF-Chem is capable of reproducing the
4 magnitude and temporal variations of VOC concentration originating from both
5 anthropogenic and biogenic sources. Specifically, modelled results tend to underestimate
6 alkene concentration but over predict aromatic level with normalized mean bias of -11% and
7 20%, similar to previous simulations for Shanghai (Tie et al., 2013). There still exist
8 substantial uncertainties in China's anthropogenic VOC emission inventory, particularly
9 speciated estimations, which was ascribed to uncertainties in the activity data, limited direct
10 experiments on emission factors and source profiles (Wei et al., 2008; Zheng et al., 2009).
11 Large biases in model-predicted aromatic level are expectable since it mainly emitted from
12 petrochemical plants, gasoline vehicle and biomass burning with greater uncertainties in
13 activity level estimation (Liu et al., 2008). In term of biogenic VOC, simplification in
14 vegetation classification and numerical descriptions, limited understanding of controlling
15 factors could introduce biases in modelled levels of BVOCs (Guenther et al., 2013). Given
16 these uncertainties, the gaps between simulation and observations in Fig. 4(a-c) are acceptable.
17 As for simulated biogenic terpenes, whose oxidation products have low vapour pressures
18 similar to sulphuric acid and condense onto aerosol surfaces, the spatial patterns in the
19 morning of the aforementioned three NPF days showed great differences (Fig. 4(d-f)). During
20 the first and third NPF cases, prevailing easterly winds did not bring much biogenic VOC
21 since biogenic emissions are most intensive in the southern part of China. By contrast, on 10
22 July when the air temperature was getting higher and southwesterly winds dominated,
23 enhanced biogenic emissions and the shift in wind direction caused that the modelled terpene
24 concentrations at the SORPES station were almost two times those in the other two NPF days.

25 3.2.2 MALTE-BOX simulations

26 Fig. 5 shows the variations of modelled particle number size distributions during the three
27 NPF days. The model system does reproduce the occurrence of these three NPF events
28 although they were under distinct meteorological conditions and affected by entirely different
29 potential source regions. On 22 June when measured air masses originated from the urbanized
30 YRD region, the calculated onset of activation of freshly formed cluster to grow above the 6
31 nm line appeared around 08:30 LT. According to the diurnal pattern of simulated
32 concentrations of gaseous compounds illustrated in Fig. 6, the OH radical level increased

1 rapidly from 1×10^5 to $3 \times 10^6 \text{ \# cm}^{-3}$ just after sunrise, promoting the gaseous oxidation of SO_2
2 in the atmosphere and subsequent accumulation of sulphuric acid from nearly zero to around
3 $5 \times 10^6 \text{ \# cm}^{-3}$. Simultaneously, the pre-existing particle concentration dropped down due to the
4 boundary layer evolution (Fig. 3). The continuously growing sulphuric acid concentration and
5 decreasing condensation sink jointly led to this fast NPF event. Simulated J_6 was $9.3 \text{ cm}^{-3} \text{ s}^{-1}$,
6 slightly higher than the observed value of $7.6 \text{ cm}^{-3} \text{ s}^{-1}$. Among different kinds of condensing
7 vapours, sulphuric acid contributed most to the growth of newly formed particles. As
8 demonstrated in Fig. 7, while considering the growth of particles less than 10 nm in diameter,
9 sulphuric acid's contribution accounted for more than 50%. The reason is that, influenced by
10 air mass from the emission-intensive YRD region, SO_2 was reaching up to 20 ppb and the
11 contribution of sulphuric acid on this day was much higher compared with the other two days
12 and those published in earlier studies (Boy et al., 2003 and 2008b). GR_{6-30} was simulated to
13 be 6.9 nm h^{-1} , about half of that derived from measurements. Overestimated newly formed
14 clusters might be one reason for smaller simulated GR_{6-30} . Another, as described before,
15 condensing vapours in the box model only included biogenic low volatile compounds.
16 However, aromatic-related oxidation products have been suspected to be contributing to
17 particle growth, especially in polluted area like China (Zhang et al., 2004; Yue et al., 2010).
18 Failing to characterize condensing vapour originating from anthropogenic organic compounds
19 might be another cause for under-predicted growth rate.

20 During the second NPF case, the OH radical concentration was mostly less than $1 \times 10^6 \text{ \# cm}^{-3}$.
21 The production of sulphuric acid was expected to be relatively slow due to the simultaneous
22 lower concentrations of both SO_2 and OH radical. As demonstrated in Fig. 6, the
23 concentration of sulphuric acid was approximately $3 \times 10^5 \text{ \# cm}^{-3}$ just when the NPF started,
24 about one-tenth and one-seventh of the corresponding values on 22 June and 22 August,
25 respectively. Nonetheless, prevailing south-westerly winds brought along terpenes-rich air
26 masses. Some of the terpenes, such as alpha-pinene and limonene, feature significantly high
27 yields of ELVOCs as well as SVOCs while reacting with ozone or OH radicals (Ehn et al.,
28 2014; Jokinen et al., 2015). Such dense low volatile oxidation products substantially enhanced
29 condensational growth of newly formed particles. The individual contributions from
30 sulphuric acid, SVOCs, ELVOCs to growth of newly formed particles were quantified in Fig.
31 7, which indicated that biogenic low volatile compounds overwhelmingly dominated in the
32 very initial stage of cluster growth with contribution as high as 95%, demonstrating a vital
33 role of ELVOCs and SVOCs in this NPF event (Ehn et al., 2014). During this event, SVOCs-

1 induced condensational growth of small clusters was especially higher, which might be
2 attributed to the fact that modelled SVOC concentrations increased dramatically shortly after
3 the nucleation started and was almost ten times higher than those during the other two events.
4 Unlike during the first two NPF cases, the level of pre-existing particles was unusually low
5 during the third event because a strong wind from the ocean swept over East China. The clean
6 air mass reduced the condensation sink (see Table 2), much lower than the values typically
7 observed at the SORPES site before (Herrmann et al., 2014). Even though SO₂ concentrations
8 were pretty low, sulphuric acid accumulated remarkably and probably initiated this NPF event.
9 As listed in Table 2, during Case 3 when the air mass originated partly over the Shanghai and
10 surrounding city clusters, the model underpredicted the growth rate nearly by a factor of 7 and
11 overestimates the particle formation rate by 3 times. This means that most probably
12 anthropogenic low volatile compounds not included in the model were contributing to the
13 growth and decreased the surviving probability of the newly formed clusters in the model. It
14 is completely opposite for Case 2 when the air mass originated not from strong anthropogenic
15 influenced areas and the model outcome was in good agreement with the measurements.

16 3.2.3 Discussions and uncertainties

17 Though the model succeeded in the prediction of DMPS-measured NPF occurrence, the
18 simulated activation of NPF was about one hour later than the observations. Considering the
19 number concentration in the size range 6-10 nm (N₆₋₁₀) as the newly formed particles, model
20 shows a distinct underestimation at the beginning of the NPF events (Fig. 5). As mentioned in
21 Sect. 2, we assumed the kinetic mechanism in the MALTE-BOX. Nonetheless, chamber and
22 in-situ experiments speculated that monoterpene oxidation products could cluster directly
23 with a single sulphuric acid molecule under ambient conditions and that the interaction
24 between organic and sulphuric acids likely leads to a reduced nucleation barrier (R. Y. Zhang
25 et al., 2004b; Schobesberger et al., 2013). Furthermore, according to the simulation, the
26 production of ELVOCs and SVOCs was mainly initialized by the reactions between
27 monoterpene and ozone. It has been recognized that NPF events tend to be strongly associated
28 with the monoterpene oxidation products by ozone in both remote and urban environments
29 (Laaksonen et al., 2008; Guo et al., 2012). Thus, there was a good chance that the ELVOCs
30 played an important part in the NPF processes considered here. As presented in Fig. 6, a
31 considerable amount of ELVOCs accumulated before modelled NPF occurred and during the
32 observed NPF events. The time shifts of the starting times is consistent with the hypothesis

1 that organic vapours may play a key role in the particle formation process (Paasonen et al.,
2 2009; Metzger et al., 2010). Fig. 8(a) shows the dependence of measurement-derived J_6 on
3 modelled gaseous sulphuric acid and ELVOC concentrations. 6 nm new particle formation
4 rates, even under the same sulphuric acid concentration, were substantially enhanced by the
5 presence of ELVOCs. It is noteworthy that formation rates of 6 nm particles, not nucleation
6 rates, are available here due to the limitation of instruments. It is hard to identify which
7 process is mostly promoted by ELVOCs, either the particle formation or the early
8 condensational growth. Metzger et al. (2010) attempted to disentangle the influence of
9 organic oxidation products in particle formation and suggested an overall dependency on the
10 formation rate of H_2SO_4 and organic oxidation products with the lowest volatility (NucOrg)
11 as listed below.

$$12 \quad J_{1.5} = k \times [H_2SO_4]^{1.0} [NucOrg]^{0.8} \quad \text{Eq. 5}$$

13 where, $J_{1.5}$ is new particle formation rate of 1.5 nm cluster; k represents pre-factor which
14 recommended to be $7.2 \pm 1.4 \times 10^{-13} \text{ cm}^3 \text{ s}^{-1}$ in Metzger et al. (2010); $[H_2SO_4]$ and $[NucOrg]$
15 refer to the concentration of sulphuric acid and low volatile organic oxidation products that
16 can participate in the particle formation process, respectively. By assuming that NucOrg is
17 part of the ELVOCs in the present work, we examined the relationships between measured
18 particle formation rate with $[H_2SO_4]^{1.0} [ELVOCs]^{0.8}$ and compared it with $[H_2SO_4]^2$ in Fig.
19 8(b-c). The better representation and correlation of the latter provides further evidence for an
20 involvement of ELVOCs in the formation and condensational growth of particles up to 6 nm.

21 In terms of the condensational growth of freshly-formed particles, ambient low-volatility
22 compounds are predominant contributors, in particular, semi-volatile and possibly non-
23 volatile organic matters generating from a complex series of photochemical reactions (Kroll
24 and Seinfeld, 2008). In the present work, the model notably underestimates the nuclei
25 condensational growth (GR_{6-30}) for Case 1 and Case 3 compared with the corresponding
26 observations, whereas the observation and simulation were comparable for the Case 2 (Table
27 2). These differences could partly be due to the fact that here we only took oxidation products
28 for certain selected organic compounds into account as sources of condensable vapours.
29 When the experimental site was substantially influenced by intensive industrial activities and
30 vehicle emissions from the YRD region in Case 1 and Case 3, reactive uptake and
31 condensable secondary organic products from anthropogenic VOCs, which can accelerate
32 particle growth (R. Y. Zhang et al., 2004b; Kroll et al., 2005; Volkamer et al., 2006), were

1 partly missing in the present model. Regarding the impacts of biogenic VOCs, we found that
2 ELVOCs and SVOCs remarkably contributed to particle condensational growth. Modelled
3 contributions from ELVOCs, SVOCs and sulphuric acid demonstrated that, during these three
4 NPF days, condensation of ELVOCs and SVOCs played an important role in the initial
5 growth of particles less than 10 nm. In particular, the contribution increased to over 90% on
6 10 July when the terpenes-rich air mass influenced the SORPES site.

7 The comprehensive modelling study on the observed new particle formation makes it possible
8 to better understand NPF processes at the SORPES station. However, there still lie many
9 uncertainties in this modelling system, which need to be improved in future work. Given the
10 expensive computational cost, reactions of VOCs are represented by the lumped mechanism
11 in the regional-scale WRF-Chem model. Relevant parameters cannot be precisely determined
12 for one lumped class, while the MALTE-BOX model provides accurate information for each
13 specific organic compound. The gaps between the two models concerning VOC classification
14 would introduce uncertainties. Moreover, in the MALTE-BOX model, sulphuric acid tends to
15 be under-predicted, which was demonstrated in both polluted urban environment and clean
16 rural environment (Wang et al., 2013a; Zhou et al., 2014; Zhou et al., 2015). There are
17 multiple reasons behind the systematic underestimation. It has been shown by field
18 measurements, laboratory experiments and numeric simulation that Crige Intermediates (CIs)
19 or other derivatives are capable of accelerating the oxidation of SO₂ into SO₃ (Hatakeyama
20 and Akimoto, 1994; Kurten et al., 2011; Boy et al., 2013). These reactions have been
21 incorporated in the MALTE-BOX model but would need further investigations concerning
22 the reactions rates and other important reaction parameters (e.g. thermal lifetimes of CIs,
23 pressure dependency, etc.). In addition, owing to the far incomplete knowledge of HONO
24 sources, in particular during daytime, it was not yet possible to simulate realistic HONO
25 levels using current models (Elshorbany et al., 2014; Czader et al., 2015). The lack of HONO
26 measurement input to the model might also result in an underestimation of sulphuric acid,
27 especially with dramatically increasing traffic emissions during the rush hours (Wang et al.,
28 2013b). For instance, in the first case, the air masses were carrying on more characteristic
29 from the emissions-intensive YRD region, the sulphuric acid concentrations and particle
30 formation rates are more likely to be under-predicted. Last but not least, we adopted a
31 mandatory value for the kinetic coefficient, which includes the probability that a collision of
32 two molecules results in the formation of a stable critical cluster, as well as all other important
33 details concerning the particle formation process such as temperature and humidity. This

1 condition-dependent coefficient needs to be resolved in further modelling work on the basis
2 of more in-situ and laboratory experiments.

3

4 **4 Conclusions**

5 This study combines the regional chemical transport model and box model to investigate
6 atmospheric new particle formation and its subsequent nuclei condensational growth at the
7 SORPES site in Nanjing, China. This combination makes it possible to simulate chemical and
8 aerosol dynamical processes. Three NPF cases, during which entirely different potential
9 source regions influenced the experimental site, were successfully reproduced by the
10 modelling system. When the site was predominately influenced by air masses from city
11 clusters in the YRD region on 22 June, 2013, despite a high condensation sink, the NPF event
12 featured fast new particle formation rate due to the continuously accumulating sulphuric acid.
13 Under the circumstance that biogenic VOC-rich air masses dominated, rapid growth of
14 freshly formed particle was detected on 10 July, 2013, which was predominately attributed to
15 the low-volatility oxidation products of terpenes. Air masses from marine origin could lead to
16 the relatively low condensation sink on 22 August, 2013, thereby facilitating the occurrence
17 of NPF event. On the basis of measurements and the corresponding modelling, we infer the
18 controlling factors of the selected three NPF events, and these were mostly associated with
19 sulphuric acid accumulation and low condensation sink. The comparison with the
20 observations suggested that low-volatility organic compounds, including both SVOCs and
21 ELVOCs, played a substantial role in the initial condensational growth of newly formed
22 particles, particularly when the station was influenced by air masses originated from the South
23 China. In addition, anthropogenic VOCs and the following photochemical oxidation produce
24 a considerable amount of condensable compounds, exerting a significant impact on particle
25 growth in the emission-intensive YRD region. Although some inadequacies still remain, such
26 as the inclusion of anthropogenic non-volatile organic compounds as condensable vapours,
27 the comprehensive modelling work provides a better insight of NPF processes.

28

29 **Acknowledgements**

30 This work was supported by the National Natural Science Foundation of China
31 (D0512/41422504, D0510/41505109, D0512/91544231 and D512/41305123), the National

1 Key Technology Research and Development Program (2014BAC22B02) and the Science and
2 Technology Support Program of Jiangsu Province (SBE2014070928). Part of this work was
3 supported by the Jiangsu Provincial Science Fund for Distinguished Young Scholars awarded
4 to A. J. Ding (No. BK20140021) and by the Academy of Finland projects (1118615, 139656)
5 and the European Commission via ERC Advanced Grant ATM-NUCLE. We also thank the
6 financial support from Helsinki University Centre of Environment (HENVI).

7

8 **References**

- 9 Almeida, J., Schobesberger, S., Kurten, A., Ortega, I. K., Kupiainen-Maatta, O., Praplan, A. P., Adamov, A.,
10 Amorim, A., Bianchi, F., Breitenlechner, M., David, A., Dommen, J., Donahue, N. M., Downard, A., Dunne, E.,
11 Duplissy, J., Ehrhart, S., Flagan, R. C., Franchin, A., Guida, R., Hakala, J., Hansel, A., Heinritzi, M., Henschel,
12 H., Jokinen, T., Junninen, H., Kajos, M., Kangasluoma, J., Keskinen, H., Kupc, A., Kurten, T., Kvashin, A. N.,
13 Laaksonen, A., Lehtipalo, K., Leiminger, M., Leppa, J., Loukonen, V., Makhmutov, V., Mathot, S., McGrath, M.
14 J., Nieminen, T., Olenius, T., Onnela, A., Petaja, T., Riccobono, F., Riipinen, I., Rissanen, M., Rondo, L.,
15 Ruuskanen, T., Santos, F. D., Sarnela, N., Schallhart, S., Schnitzhofer, R., Seinfeld, J. H., Simon, M., Sipila, M.,
16 Stozhkov, Y., Stratmann, F., Tome, A., Trostl, J., Tsagkogeorgas, G., Vaattovaara, P., Viisanen, Y., Virtanen, A.,
17 Vrtala, A., Wagner, P. E., Weingartner, E., Wex, H., Williamson, C., Wimmer, D., Ye, P. L., Yli-Juuti, T.,
18 Carslaw, K. S., Kulmala, M., Curtius, J., Baltensperger, U., Worsnop, D. R., Vehkamäki, H., and Kirkby, J.:
19 Molecular understanding of sulphuric acid-amine particle nucleation in the atmosphere, *Nature*, 502, 359-363,
20 doi:10.1038/Nature12663, 2013.
- 21 Boy, M., Rannik, U., Lehtinen, K. E. J., Tarvainen, V., Hakola, H., and Kulmala, M.: Nucleation events in the
22 continental boundary layer: Long-term statistical analyses of aerosol relevant characteristics, *J. Geophys. Res.*
23 *Atmos.*, 108, Artn 4667, doi:10.1029/2003jd003838, 2003.
- 24 Boy, M., Hellmuth, O., Korhonen, H., Nilsson, E. D., ReVelle, D., Turnipseed, A., Arnold, F., and Kulmala, M.:
25 MALTE - model to predict new aerosol formation in the lower troposphere, *Atmos. Chem. Phys.*, 6, 4499-4517,
26 2006.
- 27 Boy, M., Bonn, B., Kazil, J., Lovejoy, N., Turnipseed, A., Greenberg, J., Karl, T., Mauldin, L., Kuciuch, E., and
28 Smith, J.: Relevance of several nucleation theories in different environments, in: *Nucleation and Atmospheric*
29 *Aerosols*, Springer, 87-91, 2007.
- 30 Boy, M., Kazil, J., Lovejoy, E. R., Guenther, A., and Kulmala, M.: Relevance of ion-induced nucleation of
31 sulfuric acid and water in the lower troposphere over the boreal forest at northern latitudes, *Atmos. Res.*, 90,
32 151-158, 2008a.
- 33 Boy, M., Karl, T. , Turnipseed, A., Mauldin, L., Kosciuch, E., Greenberg, J., Rathbone, J., Smith, J., Held, A.,
34 Barsanti, K., Wehner, B., Bauer, S., Wiedensohler, A., Bonn, B., Kulmala, M. and Guenther, A.: New particle
35 formation at the Front Range of the Colorado Rockies, *Atmos. Chem. Phys.*, 8, 1577-1590, 2008b.

1 Boy, M., Mogensen, D., Smolander, S., Zhou, L., Nieminen, T., Paasonen, P., Plass-Dulmer, C., Sipila, M.,
2 Petaja, T., Mauldin, L., Berresheim, H., and Kulmala, M.: Oxidation of SO₂ by stabilized Criegee intermediate
3 (sCI) radicals as a crucial source for atmospheric sulfuric acid concentrations, *Atmos. Chem. Phys.*, 13, 3865-
4 3879, doi:10.5194/acp-13-3865-2013, 2013.

5 Carter W. P. L. Documentation of the SAPRC-99 chemical mechanism for VOC reactivity assessment,
6 University of California, Riverside, CA, 446 pp.,1999.

7 Czader, B., Choi, Y., Li, X., Alvarez, S., and Lefer, B.: Impact of updated traffic emissions on HONO mixing
8 ratios simulated for urban site in Houston, Texas, *Atmos. Chem. Phys.*, 15, 1253-1263, 2015.

9 Damian, V., Sandu, A., Damian, M., Potra, F., and Carmichael, G. R.: The kinetic preprocessor KPP - a software
10 environment for solving chemical kinetics, *Comput Chem Eng*, 26, 1567-1579, 2002.

11 Davidson, C. I., Phalen, R. F., and Solomon, P. A.: Airborne particulate matter and human health: A review,
12 *Aerosol Sci. Tech.*, 39, 737-749, doi:10.1080/02786820500191348, 2005.

13 Ding, A. J., Fu, C. B., Yang, X. Q., Sun, J. N., Zheng, L. F., Xie, Y. N., Herrmann, E., Nie, W., Petaja, T.,
14 Kerminen, V. M., and Kulmala, M.: Ozone and fine particle in the western Yangtze River Delta: an overview of
15 1 yr data at the SORPES station, *Atmos. Chem. Phys.*, 13, 5813-5830, doi:10.5194/acp-13-5813-2013, 2013a.

16 Ding, A. J., Fu, C. B., Yang, X. Q., Sun, J. N., Petaja, T., Kerminen, V. M., Wang, T., Xie, Y., Herrmann, E.,
17 Zheng, L. F., Nie, W., Liu, Q., Wei, X. L., and Kulmala, M.: Intense atmospheric pollution modifies weather: a
18 case of mixed biomass burning with fossil fuel combustion pollution in eastern China, *Atmos. Chem. Phys.*, 13,
19 10545-10554, doi:10.5194/acp-13-10545-2013, 2013b.

20 Ding, A. J., Wang, T., and Fu, C. B.: Transport characteristics and origins of carbon monoxide and ozone in
21 Hong Kong, South China, *J Geophys Res-Atmos*, 118, 9475-9488, 10.1002/jgrd.50714, 2013c.

22 Ehn, M., Thornton, J. A., Kleist, E., Sipila, M., Junninen, H., Pullinen, I., Springer, M., Rubach, F., Tillmann, R.,
23 Lee, B., Lopez-Hilfiker, F., Andres, S., Acir, I. H., Rissanen, M., Jokinen, T., Schobesberger, S., Kangasluoma,
24 J., Kontkanen, J., Nieminen, T., Kurten, T., Nielsen, L. B., Jorgensen, S., Kjaergaard, H. G., Canagaratna, M.,
25 Dal Maso, M., Berndt, T., Petaja, T., Wahner, A., Kerminen, V. M., Kulmala, M., Worsnop, D. R., Wildt, J., and
26 Mentel, T. F.: A large source of low-volatility secondary organic aerosol, *Nature*, 506, 476-479,
27 doi:10.1038/Nature13032, 2014.

28 Eidels-Dubovoi, S.: Aerosol impacts on visible light extinction in the atmosphere of Mexico City, *Sci. Total*
29 *Environ.*, 287, 213-220, doi:10.1016/S0048-9697(01)00983-4, 2002.

30 Ek, M. B., Mitchell, K. E., Lin, Y., Rogers, E., Grunmann, P., Koren, V., Gayno, G., and Tarpley, J. D.:
31 Implementation of Noah land surface model advances in the National Centers for Environmental Prediction
32 operational mesoscale Eta model, *J. Geophys. Res. Atmos.*, 108, Artn 8851, doi:10.1029/2002jd003296, 2003.

33 Elshorbany, Y. F., Crutzen, P. J., Steil, B., Pozzer, A., Tost, H., and Lelieveld, J.: Global and regional impacts of
34 HONO on the chemical composition of clouds and aerosols, *Atmos. Chem. Phys.*, 14, 1167-1184,
35 doi:10.5194/acp-14-1167-2014, 2014.

1 Gao, J., Wang, T., Zhou, X. H., Wu, W. S., and Wang, W. X.: Measurement of aerosol number size distributions
2 in the Yangtze River delta in China: Formation and growth of particles under polluted conditions, *Atmos.*
3 *Environ.*, 43, 829-836, doi:10.1016/j.atmosenv.2008.10.046, 2009.

4 Gao, J., Chai, F. H., Wang, T., and Wang, W. X.: Particle number size distribution and new particle formation
5 (NPF) in Lanzhou, Western China, *Particuology*, 9, 611-618, doi:10.1016/j.partic.2011.06.008, 2011.

6 Gao, J., Chai, F. H., Wang, T., Wang, S. L., and Wang, W. X.: Particle number size distribution and new particle
7 formation: New characteristics during the special pollution control period in Beijing, *J. Environ. Sci-China*, 24,
8 14-21, doi:10.1016/S1001-0742(11)60725-0, 2012.

9 Grell, G. A., and Devenyi, D.: A generalized approach to parameterizing convection combining ensemble and
10 data assimilation techniques, *Geophys. Res. Lett.*, 29, Artn 1693, doi:10.1029/2002gl015311, 2002.

11 Grell, G. A., Peckham, S. E., Schmitz, R., McKeen, S. A., Frost, G., Skamarock, W. C., and Eder, B.: Fully
12 coupled "online" chemistry within the WRF model, *Atmos. Environ.*, 39, 6957-6975, 2005.

13 Guenther, A., Karl, T., Harley, P., Wiedinmyer, C., Palmer, P. I., and Geron, C.: Estimates of global terrestrial
14 isoprene emissions using MEGAN (Model of Emissions of Gases and Aerosols from Nature), *Atmos. Chem.*
15 *Phys.*, 6, 3181-3210, 2006.

16 Guenther, A.: Biological and chemical diversity of biogenic volatile organic emissions into the atmosphere,
17 *ISRN Atmos. Sci.*, 2013, 2013.

18 Guo, H., Wang, D. W., Cheung, K., Ling, Z. H., Chan, C. K., and Yao, X. H.: Observation of aerosol size
19 distribution and new particle formation at a mountain site in subtropical Hong Kong, *Atmos. Chem. Phys.*, 12,
20 9923-9939, doi:10.5194/acp-12-9923-2012, 2012.

21 Guo, S., Hu, M., Zamora, M. L., Peng, J. F., Shang, D. J., Zheng, J., Du, Z. F., Wu, Z., Shao, M., Zeng, L. M.,
22 Molina, M. J., and Zhang, R. Y.: Elucidating severe urban haze formation in China, *Proc. Natl. Acad. Sci. U. S.*
23 *A.*, 111, 17373-17378, doi:10.1073/pnas.1419604111, 2014.

24 Hatakeyama, S., and Akimoto, H.: Reactions of Criegee Intermediates in the Gas-Phase, *Res. Chem. Intermediat.*,
25 20, 503-524, doi:10.1163/156856794x00432, 1994.

26 Herrmann, E., Ding, A. J., Kerminen, V. M., Petaja, T., Yang, X. Q., Sun, J. N., Qi, X. M., Manninen, H.,
27 Hakala, J., Nieminen, T., Aalto, P. P., Kulmala, M., and Fu, C. B.: Aerosols and nucleation in eastern China:
28 first insights from the new SORPES-NJU station, *Atmos. Chem. Phys.*, 14, 2169-2183, doi:10.5194/acp-14-
29 2169-2014, 2014.

30 Hildemann, L. M., Russell, A. G., and Cass, G. R.: Ammonia and nitric-acid concentrations in equilibrium with
31 atmospheric aerosols - experiment vs theory, *Atmos. Environ.*, 18, 1737-1750, 1984.

32 Hong, S. Y.: A new stable boundary-layer mixing scheme and its impact on the simulated East Asian summer
33 monsoon, *Q. J. R. Meteorol. Soc.*, 136, 1481-1496, doi:10.1002/Qj.665, 2010.

1 Huang, X., Song, Y., Zhao, C., Li, M. M., Zhu, T., Zhang, Q., and Zhang, X. Y.: Pathways of sulfate
2 enhancement by natural and anthropogenic mineral aerosols in China, *J. Geophys. Res. Atmos.*, 119, 14165-
3 14179, doi:10.1002/2014jd022301, 2014.

4 Huang, X., Song, Y., Zhao, C., Cai, X. H., Zhang, H. S., and Zhu, T.: Direct Radiative Effect by
5 Multicomponent Aerosol over China, *J. Climate*, 28, 3472-3495, doi:10.1175/Jcli-D-14-00365.1, 2015.

6 Jokinen, T., Berndt, T., Makkonen, R., Kerminen, V. M., Junninen, H., Paasonen, P., Stratmann, F., Herrmann,
7 H., Guenther, A. B., Worsnop, D. R., Kulmala, M., Ehn, M., and Sipila, M.: Production of extremely low
8 volatile organic compounds from biogenic emissions: Measured yields and atmospheric implications, *Proc. Nat.*
9 *Acad. Sci. U. S. A.*, 112, 7123-7128, doi:10.1073/pnas.1423977112, 2015.

10 Kerminen, V. M., and Wexler, A. S.: The occurrence of sulfuric acid-water nucleation in plumes: Urban
11 environment, *Tellus B*, 48, 65-82, doi:10.1034/j.1600-0889.1996.00007.x, 1996.

12 Kerminen, V. M., Paramonov, M., Anttila, T., Riipinen, I., Fountoukis, C., Korhonen, H., Asmi, E., Laakso, L.,
13 Lihavainen, H., Swietlicki, E., Svenningsson, B., Asmi, A., Pandis, S. N., Kulmala, M., and Petaja, T.: Cloud
14 condensation nuclei production associated with atmospheric nucleation: a synthesis based on existing literature
15 and new results, *Atmos. Chem. Phys.*, 12, 12037-12059, doi:10.5194/acp-12-12037-2012, 2012.

16 Korhonen, P., Kulmala, M., Laaksonen, A., Viisanen, Y., McGraw, R., and Seinfeld, J. H.: Ternary nucleation of
17 H₂SO₄, NH₃, and H₂O in the atmosphere, *J. Geophys. Res. Atmos.*, 104, 26349-26353, doi:
18 10.1029/1999jd900784, 1999.

19 Kroll, J. H., Ng, N. L., Murphy, S. M., Varutbangkul, V., Flagan, R. C., and Seinfeld, J. H.: Chamber studies of
20 secondary organic aerosol growth by reactive uptake of simple carbonyl compounds, *J. Geophys. Res. Atmos.*,
21 110, Artn D23207, doi:10.1029/2005jd006004, 2005.

22 Kroll, J. H., and Seinfeld, J. H.: Chemistry of secondary organic aerosol: Formation and evolution of low-
23 volatility organics in the atmosphere, *Atmos. Environ.*, 42, 3593-3624, doi:10.1016/j.atmosenv.2008.01.003,
24 2008.

25 Kulmala, M., Kerminen, V.-M., and Laaksonen, A.: Simulations on the effect of sulphuric acid formation on
26 atmospheric aerosol concentrations, *Atmos. Environ.*, 29, 377-382, 1995.

27 Kulmala, M., Dal Maso, M., Makela, J. M., Pirjola, L., Vakeva, M., Aalto, P., Miiikkulainen, P., Hameri, K., and
28 O'Dowd, C. D.: On the formation, growth and composition of nucleation mode particles, *Tellus B*, 53, 479-490,
29 doi:10.1034/j.1600-0889.2001.530411.x, 2001.

30 Kulmala, M., Suni, T., Lehtinen, K. E. J., Dal Maso, M., Boy, M., Reissell, A., Rannik, U., Aalto, P., Keronen,
31 P., Hakola, H., Back, J. B., Hoffmann, T., Vesala, T., and Hari, P.: A new feedback mechanism linking forests,
32 aerosols, and climate, *Atmos. Chem. Phys.*, 4, 557-562, 2004a.

33 Kulmala, M., Vehkamaki, H., Petaja, T., Dal Maso, M., Lauri, A., Kerminen, V. M., Birmili, W., and McMurry,
34 P. H.: Formation and growth rates of ultrafine atmospheric particles: a review of observations, *J. Aerosol. Sci.*,
35 35, 143-176, doi:10.1016/j.jaerosci.2003.10.003, 2004b.

1 Kulmala, M., and Kerminen, V. M.: On the formation and growth of atmospheric nanoparticles, *Atmos. Res.*, 90,
2 132-150, doi:10.1016/j.atmosres.2008.01.005, 2008.

3 Kulmala, M., Petaja, T., Nieminen, T., Sipila, M., Manninen, H. E., Lehtipalo, K., Dal Maso, M., Aalto, P. P.,
4 Junninen, H., Paasonen, P., Riipinen, I., Lehtinen, K. E. J., Laaksonen, A., and Kerminen, V. M.: Measurement
5 of the nucleation of atmospheric aerosol particles, *Nat. Protoc.*, 7, 1651-1667, doi:10.1038/nprot.2012.091, 2012.

6 Kurten, T., Lane, J. R., Jorgensen, S., and Kjaergaard, H. G.: A Computational Study of the Oxidation of SO₂ to
7 SO₃ by Gas-Phase Organic Oxidants, *J. Phys. Chem. A*, 115, 8669-8681, doi:10.1021/Jp203907d, 2011.

8 Laaksonen, A., Kulmala, M., O'Dowd, C. D., Joutsensaari, J., Vaattovaara, P., Mikkonen, S., Lehtinen, K. E. J.,
9 Sogacheva, L., Dal Maso, M., Aalto, P., Petaja, T., Sogachev, A., Yoon, Y. J., Lihavainen, H., Nilsson, D.,
10 Facchini, M. C., Cavalli, F., Fuzzi, S., Hoffmann, T., Arnold, F., Hanke, M., Sellegri, K., Umann, B.,
11 Junkermann, W., Coe, H., Allan, J. D., Alfarra, M. R., Worsnop, D. R., Riekkola, M. L., Hyotylainen, T., and
12 Viisanen, Y.: The role of VOC oxidation products in continental new particle formation, *Atmos. Chem. Phys.*, 8,
13 2657-2665, 2008.

14 Li, M., Huang, X., Li, J., and Song, Y.: Estimation of biogenic volatile organic compound (BVOC) emissions
15 from the terrestrial ecosystem in China using real-time remote sensing data, *Atmos. Chem. Phys. Discuss.*, 12,
16 6551-6592, 2012.

17 Lihavainen, H., Kerminen, V. M., Komppula, M., Hatakka, J., Aaltonen, V., Kulmala, M., and Viisanen, Y.:
18 Production of "potential" cloud condensation nuclei associated with atmospheric new-particle formation in
19 northern Finland, *J Geophys. Res. Atmos.*, 108, Artn 4782, doi:10.1029/2003jd003887, 2003.

20 Lin, Y. L., Farley, R. D., and Orville, H. D.: Bulk Parameterization of the Snow Field in a Cloud Model, *J. Clim.*
21 *Appl. Meteorol.*, 22, 1065-1092, doi:10.1175/1520-0450(1983)022<1065:Bpotsf>2.0.Co;2, 1983.

22 Liu, Y., Shao, M., Fu, L. L., Lu, S. H., Zeng, L. M., and Tang, D. G.: Source profiles of volatile organic
23 compounds (VOCs) measured in China: Part I, *Atmos. Environ.*, 42, 6247-6260, doi:10.1016/j.atmosenv.
24 2008.01.070, 2008.

25 Liu, S., Hu, M., Wu, Z. J., Wehner, B., Wiedensohler, A., and Cheng, Y. F.: Aerosol number size distribution
26 and new particle formation at a rural/coastal site in Pearl River Delta (PRD) of China, *Atmos. Environ.*, 42,
27 6275-6283, doi:10.1016/j.atmosenv.2008.01.063, 2008.

28 Liu, Y., Shao, M., Fu, L. L., Lu, S. H., Zeng, L. M., and Tang, D. G.: Source profiles of volatile organic
29 compounds (VOCs) measured in China: Part I, *Atmos. Environ.*, 42, 6247-6260,
30 doi:10.1016/j.atmosenv.2008.01.070, 2008.

31 Lohmann, U., and Feichter, J.: Global indirect aerosol effects: a review, *Atmos. Chem. Phys.*, 5, 715-737, 2005.

32 Makkonen, R., Asmi, A., Kerminen, V. M., Boy, M., Arneth, A., Hari, P., and Kulmala, M.: Air pollution
33 control and decreasing new particle formation lead to strong climate warming, *Atmos. Chem. Phys.*, 12, 1515-
34 1524, doi:10.5194/acp-12-1515-2012, 2012.

1 Merikanto, J., Spracklen, D. V., Mann, G. W., Pickering, S. J., and Carslaw, K. S.: Impact of nucleation on
2 global CCN, *Atmos. Chem. Phys.*, 9, 8601-8616, doi:10.5194/acp-9-8601-2009, 2009.

3 Metzger, A., Verheggen, B., Dommen, J., Duplissy, J., Prevot, A. S. H., Weingartner, E., Riipinen, I., Kulmala,
4 M., Spracklen, D. V., Carslaw, K. S., and Baltensperger, U.: Evidence for the role of organics in aerosol particle
5 formation under atmospheric conditions, *Proc. Natl. Acad. Sci. U. S. A.*, 107, 6646-6651,
6 doi:10.1073/pnas.0911330107, 2010.

7 Mlawer, E. J., Taubman, S. J., Brown, P. D., Iacono, M. J., and Clough, S. A.: Radiative transfer for
8 inhomogeneous atmospheres: RRTM, a validated correlated-k model for the longwave, *J. Geophys. Res. Atmos.*,
9 102, 16663-16682, doi:10.1029/97jd00237, 1997.

10 Myhre, G., Samset, B. H., Schulz, M., Balkanski, Y., Bauer, S., Berntsen, T. K., Bian, H., Bellouin, N., Chin, M.,
11 Diehl, T., Easter, R. C., Feichter, J., Ghan, S. J., Hauglustaine, D., Iversen, T., Kinne, S., Kirkevåg, A.,
12 Lamarque, J. F., Lin, G., Liu, X., Lund, M. T., Luo, G., Ma, X., van Noije, T., Penner, J. E., Rasch, P. J., Ruiz,
13 A., Seland, O., Skeie, R. B., Stier, P., Takemura, T., Tsigaridis, K., Wang, P., Wang, Z., Xu, L., Yu, H., Yu, F.,
14 Yoon, J. H., Zhang, K., Zhang, H., and Zhou, C.: Radiative forcing of the direct aerosol effect from AeroCom
15 Phase II simulations, *Atmos. Chem. Phys.*, 13, 1853-1877, doi:10.5194/acp-13-1853-2013, 2013.

16 Nannoolal, Y., Rarey, J., and Ramjugernath, D.: Estimation of pure component properties - Part 3. Estimation of
17 the vapor pressure of non-electrolyte organic compounds via group contributions and group interactions, *Fluid
18 Phase Equilib.*, 269, 117-133, doi:10.1016/j.fluid.2008.04.020, 2008.

19 O'Dowd, C. D., Jimenez, J. L., Bahreini, R., Flagan, R. C., Seinfeld, J. H., Hameri, K., Pirjola, L., Kulmala, M.,
20 Jennings, S. G., and Hoffmann, T.: Marine aerosol formation from biogenic iodine emissions, *Nature*, 417, 632-
21 636, doi:10.1038/Nature00775, 2002.

22 Ortega, I. K., Suni, T., Boy, M., Gronholm, T., Manninen, H. E., Nieminen, T., Ehn, M., Junninen, H., Hakola,
23 H., Hellen, H., Valmari, T., Arvela, H., Zegelin, S., Hughes, D., Kitchen, M., Cleugh, H., Worsnop, D. R.,
24 Kulmala, M., and Kerminen, V. M.: New insights into nocturnal nucleation, *Atmos. Chem. Phys.*, 12, 4297-4312,
25 2012.

26 Paasonen, P., Nieminen, T., Asmi, E., Manninen, H. E., Petaja, T., Plass-Dulmer, C., Flentje, H., Birmili, W.,
27 Wiedensohler, A., Horrak, U., Metzger, A., Hamed, A., Laaksonen, A., Facchini, M. C., Kerminen, V. M., and
28 Kulmala, M.: On the roles of sulphuric acid and low-volatility organic vapours in the initial steps of atmospheric
29 new particle formation, *Atmos. Chem. Phys.*, 10, 11223-11242, 10.5194/acp-10-11223-2010, 2010.

30 Paasonen, P., Sihto, S. L., Nieminen, T., Vuollekoski, H., Riipinen, I., Plass-Dulmer, C., Berresheim, H., Birmili,
31 W., and Kulmala, M.: Connection between new particle formation and sulphuric acid at Hohenpeissenberg
32 (Germany) including the influence of organic compounds, *Boreal Environ. Res.*, 14, 616-629, 2009.

33 Petaja, T., Mauldin, R. L., Kosciuch, E., McGrath, J., Nieminen, T., Paasonen, P., Boy, M., Adamov, A.,
34 Kotiaho, T., and Kulmala, M.: Sulfuric acid and OH concentrations in a boreal forest site, *Atmos. Chem. Phys.*,
35 9, 7435-7448, 2009.

1 Qi, X. M., Ding, A. J., Nie, W., Petäjä, T., Kerminen, V.-M., Herrmann, E., Xie, Y. N., Zheng, L. F., Manninen,
2 H., Aalto, P., Sun, J. N., Xu, Z. N., Chi, X. G., Huang, X., Boy, M., Virkkula, A., Yang, X.-Q., Fu, C. B., and
3 Kulmala, M.: Aerosol size distribution and new particle formation in the western Yangtze River Delta of China:
4 2 years of measurements at the SORPES station, *Atmos. Chem. Phys.*, 15, 12445-12464, doi:10.5194/acp-15-
5 12445-2015, 2015.

6 Rattigan, O., Boniface, J., Swartz, E., Davidovits, P., Jayne, J., Kolb, C., and Worsnop, D.: Uptake of gas -
7 phase SO₂ in aqueous sulfuric acid: Oxidation by H₂O₂, O₃, and HONO, *J. Geophys. Res. Atmos*, 105, 29065-
8 29078, 2000.

9 Schobesberger, S., Junninen, H., Bianchi, F., Lonn, G., Ehn, M., Lehtipalo, K., Dommen, J., Ehrhart, S., Ortega,
10 I. K., Franchin, A., Nieminen, T., Riccobono, F., Hutterli, M., Duplissy, J., Almeida, J., Amorim, A.,
11 Breitenlechner, M., Downard, A. J., Dunne, E. M., Flagan, R. C., Kajos, M., Keskinen, H., Kirkby, J., Kupc, A.,
12 Kurten, A., Kurten, T., Laaksonen, A., Mathot, S., Onnela, A., Praplan, A. P., Rondo, L., Santos, F. D.,
13 Schallhart, S., Schnitzhofer, R., Sipila, M., Tome, A., Tsagkogeorgas, G., Vehkamäki, H., Wimmer, D.,
14 Baltensperger, U., Carslaw, K. S., Curtius, J., Hansel, A., Petaja, T., Kulmala, M., Donahue, N. M., and
15 Worsnop, D. R.: Molecular understanding of atmospheric particle formation from sulfuric acid and large
16 oxidized organic molecules, *Proc. Natl. Acad. Sci. U. S. A.*, 110, 17223-17228, doi:10.1073/pnas.1306973110,
17 2013.

18 Scott, C. E., Rap, A., Spracklen, D. V., Forster, P. M., Carslaw, K. S., Mann, G. W., Pringle, K. J., Kivekas, N.,
19 Kulmala, M., Lihavainen, H., and Tunved, P.: The direct and indirect radiative effects of biogenic secondary
20 organic aerosol, *Atmos. Chem. Phys.*, 14, 447-470, doi:10.5194/acp-14-447-2014, 2014.

21 Sihto, S. L., Kulmala, M., Kerminen, V. M., Dal Maso, M., Petaja, T., Riipinen, I., Korhonen, H., Arnold, F.,
22 Janson, R., Boy, M., Laaksonen, A., and Lehtinen, K. E. J.: Atmospheric sulphuric acid and aerosol formation:
23 implications from atmospheric measurements for nucleation and early growth mechanisms, *Atmos. Chem. Phys.*,
24 6, 4079-4091, 2006.

25 Sipila, M., Berndt, T., Petaja, T., Brus, D., Vanhanen, J., Stratmann, F., Patokoski, J., Mauldin, R. L., Hyvarinen,
26 A. P., Lihavainen, H., and Kulmala, M.: The Role of Sulfuric Acid in Atmospheric Nucleation, *Science*, 327,
27 1243-1246, doi:10.1126/science.1180315, 2010.

28 Tie, X., Geng, F., Guenther, A., Cao, J., Greenberg, J., Zhang, R., Apel, E., Li, G., Weinheimer, A., Chen, J., and
29 Cai, C.: Megacity impacts on regional ozone formation: observations and WRF-Chem modeling for the
30 MIRAGE-Shanghai field campaign, *Atmos Chem Phys*, 13, 5655-5669, doi:10.5194/acp-13-5655-2013, 2013.

31 Volkamer, R., Jimenez, J. L., San Martini, F., Dzepina, K., Zhang, Q., Salcedo, D., Molina, L. T., Worsnop, D.
32 R., and Molina, M. J.: Secondary organic aerosol formation from anthropogenic air pollution: Rapid and higher
33 than expected, *Geophys. Res. Lett.*, 33, Artn L17811, doi:10.1029/2006gl026899, 2006.

34 Wang, M. and Penner, J. E.: Aerosol indirect forcing in a global model with particle nucleation, *Atmos. Chem.*
35 *Phys.*, 9, 239-260, doi:10.5194/acp-9-239-2009, 2009.

1 Wang, H. L., Zhu, B., Shen, L. J., An, J. L., Yin, Y., and Kang, H. Q.: Number size distribution of aerosols at Mt.
2 Huang and Nanjing in the Yangtze River Delta, China: Effects of air masses and characteristics of new particle
3 formation, *Atmos. Res.*, 150, 42-56, doi:10.1016/j.atmosres.2014.07.020, 2014.

4 Wang, Z., Hu, M., Wu, Z., Yue, D., Zheng, J., Zhang, R., Pei, X., Paasonen, P., Maso, M. D., and Boy, M.:
5 Investigation of the connections between atmospheric new particle formation and organics at an urban site of
6 Beijing, *Atmos. Chem. Phys. Discuss.*, 13, 3419-3450, 2013a.

7 Wang, Z. B., Hu, M., Mogensen, D., Yue, D. L., Zheng, J., Zhang, R. Y., Liu, Y., Yuan, B., Li, X., Shao, M.,
8 Zhou, L., Wu, Z. J., Wiedensohler, A., and Boy, M.: The simulations of sulfuric acid concentration and new
9 particle formation in an urban atmosphere in China, *Atmos. Chem. Phys.*, 13, 11157-11167, doi:10.5194/acp-13-
10 11157-2013, 2013b.

11 Weber, R. J., McMurry, P. H., Mauldin, R. L., Tanner, D. J., Eisele, F. L., Clarke, A. D., and Kapustin, V. N.:
12 New particle formation in the remote troposphere: A comparison of observations at various sites, *Geophys. Res.*
13 *Lett.*, 26, 307-310, doi:10.1029/1998gl900308, 1999.

14 Wei, W., Wang, S. X., Chatani, S., Klimont, Z., Cofala, J., and Hao, J. M.: Emission and speciation of non-
15 methane volatile organic compounds from anthropogenic sources in China, *Atmos. Environ.*, 42, 4976-4988,
16 doi:10.1016/j.atmosenv.2008.02.044, 2008.

17 Wu, Z. J., Hu, M., Lin, P., Liu, S., Wehner, B., and Wiedensohler, A.: Particle number size distribution in the
18 urban atmosphere of Beijing, China, *Atmos. Environ.*, 42, 7967-7980, doi:10.1016/j.atmosenv.2008.06.022,
19 2008.

20 Xiao, S., Wang, M., Yao, L., Kulmala, M., Zhou, B., Yang, X., Chen, J., Wang, D., Fu, Q., and Worsnop, D.:
21 Strong atmospheric new particle formation in winter in urban Shanghai, China, *Atmos. Chem. Phys.*, 15, 1769-
22 1781, 2015.

23 Yli-Juuti, T., Nieminen, T., Hirsikko, A., Aalto, P. P., Asmi, E., Horrak, U., Manninen, H. E., Patokoski, J., Dal
24 Maso, M., Petaja, T., Rinne, J., Kulmala, M., and Riipinen, I.: Growth rates of nucleation mode particles in
25 Hyytiälä during 2003-2009: variation with particle size, season, data analysis method and ambient conditions,
26 *Atmos. Chem. Phys.*, 11, 12865-12886, doi:10.5194/acp-11-12865-2011, 2011.

27 Yu, F., and Luo, G.: Simulation of particle size distribution with a global aerosol model: contribution of
28 nucleation to aerosol and CCN number concentrations, *Atmos. Chem. Phys.*, 9, 7691-7710, 2009.

29 Yue, D. L., Hu, M., Zhang, R. Y., Wang, Z. B., Zheng, J., Wu, Z. J., Wiedensohler, A., He, L. Y., Huang, X. F.,
30 and Zhu, T.: The roles of sulfuric acid in new particle formation and growth in the mega-city of Beijing, *Atmos.*
31 *Chem. Phys.*, 10, 4953-4960, doi:10.5194/acp-10-4953-2010, 2010.

32 Zhang, Q., Stanier, C. O., Canagaratna, M. R., Jayne, J. T., Worsnop, D. R., Pandis, S. N., and Jimenez, J. L.:
33 Insights into the chemistry of new particle formation and growth events in Pittsburgh based on aerosol mass
34 spectrometry, *Environ. Sci. Technol.*, 38, 4797-4809, doi:10.1021/Es035417u, 2004.

1 Zhang, R. Y., Suh, I., Zhao, J., Zhang, D., Fortner, E. C., Tie, X. X., Molina, L. T., and Molina, M. J.:
2 Atmospheric new particle formation enhanced by organic acids, *Science*, 304, 1487-1490,
3 doi:10.1126/science.1095139, 2004.

4 Zheng, J. Y., Zhang, L. J., Che, W. W., Zheng, Z. Y., and Yin, S. S.: A highly resolved temporal and spatial air
5 pollutant emission inventory for the Pearl River Delta region, China and its uncertainty assessment, *Atmos.*
6 *Environ.*, 43, 5112-5122, doi:10.1016/j.atmosenv.2009.04.060, 2009.

7 Zhou, L., Gierens, R., Sogachev, A., Mogensen, D., Ortega, J., Smith, J. N., Harley, P. C., Prenni, A. J., Levin, E.
8 J. T., Turnipseed, A., Rusanen, A., Smolander, S., Guenther, A. B., Kulmala, M., Karl, T., and Boy, M.:
9 Contribution from biogenic organic compounds to particle growth during the 2010 BEACHON-ROCS campaign
10 in a Colorado temperate needle leaf forest, *Atmos. Chem. Phys.*, 15, 8643–8656, doi:10.5194/acp-15-8643-2015,
11 2015

12 Zhou, L. X., Nieminen, T., Mogensen, D., Smolander, S., Rusanen, A., Kulmala, M., and Boy, M.: SOSAA - a
13 new model to simulate the concentrations of organic vapours, sulphuric acid and aerosols inside the ABL - Part 2:
14 Aerosol dynamics and one case study at a boreal forest site, *Boreal Environ. Res.*, 19, 237-256, 2014.

15

1 Table 1. Chemical species from WRF-Chem inputted to MALTE-BOX

WRF-Chem	MALTE-BOX
Acetaldehyde (CCHO)	CH3CHO
Acetone (ACET)	CH3COCH3
Methanol (MEOH)	CH3OH
Methyl Vinyl Ketone (MVK)	MVK
Isoprene (ISOPRENE)	C5H8
Terpenes (TERP)	alpha-pinene
	beta-pinene
	camphene
	myrcene
	limonene

2

3

1 Table 2. Formation rate of 6-nm particles (J_6), and particle growth rates from 6 to 30 nm
 2 (GR_{6-30}) of 3 NPF events based on DMPS measurements and numeric modelling^a.

	Date	J_6 ($\text{cm}^{-3} \text{s}^{-1}$)	GR_{6-30} (nm h^{-1})	CS (10^{-2}s^{-1})
Case1	20130622	7.6(9.3)	12.6(6.9)	4.2
Case2	20130710	1.2(1.6)	13.5(10.7)	3.2
Case3	20130822	3.4(10.0)	15.7(2.3)	1.9

3 ^avalues out of the parentheses are observations and those in the parentheses represent the
 4 corresponding model results.

5

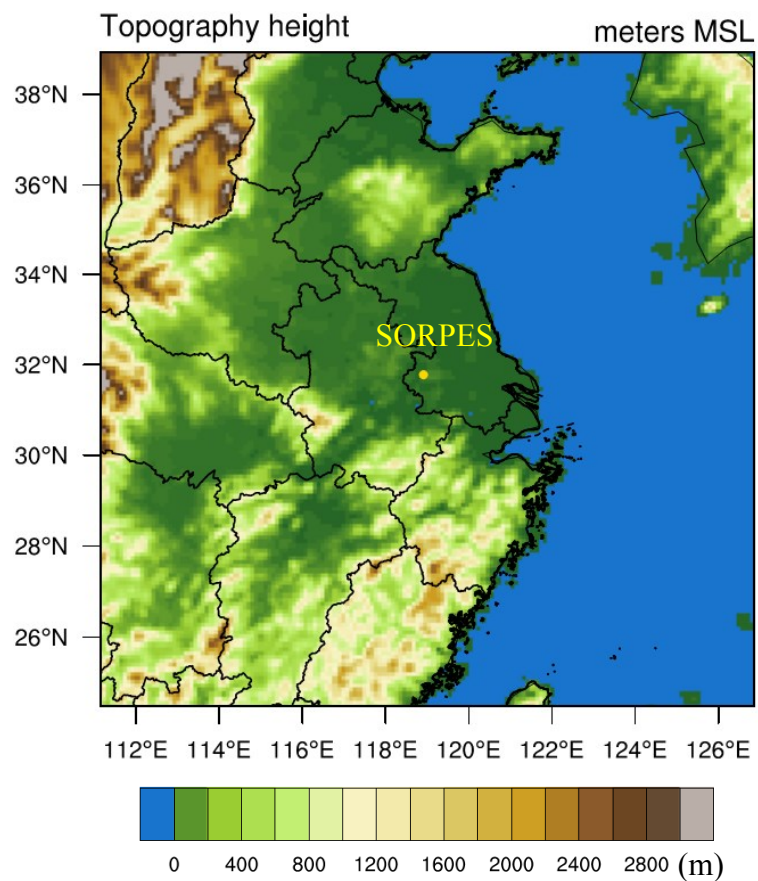
6 Table 3. Statistical analysis of the simulated hourly 2-m temperature and 10-m wind speed
 7 versus the ground observations at the SORPES station

Date	Index ^a	2-m temperature ($^{\circ}\text{C}$)	10-m wind speed (m/s)
22 June	MB	-0.33	0.80
	RMSE	1.29	1.63
10 July	MB	-1.07	-0.77
	RMSE	1.34	1.18
22 August	MB	0.19	0.17
	RMSE	1.38	1.27

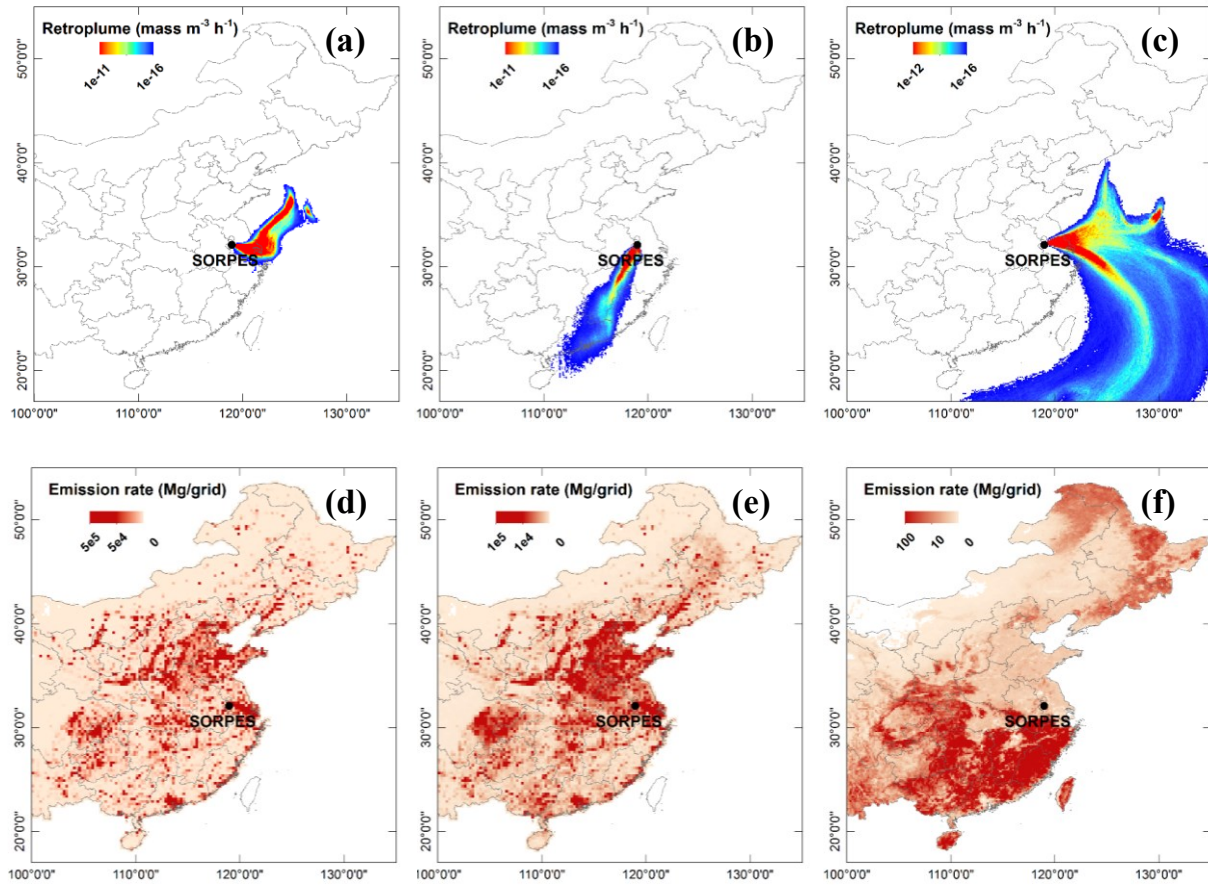
8 ^aMB and RMSE refer to mean bias and root mean square error respectively.

9

10



- 1
- 2 Figure 1. WRF-Chem model domain and topographic field (meter). The yellow dot marks the
- 3 location of the SORPESstation.
- 4

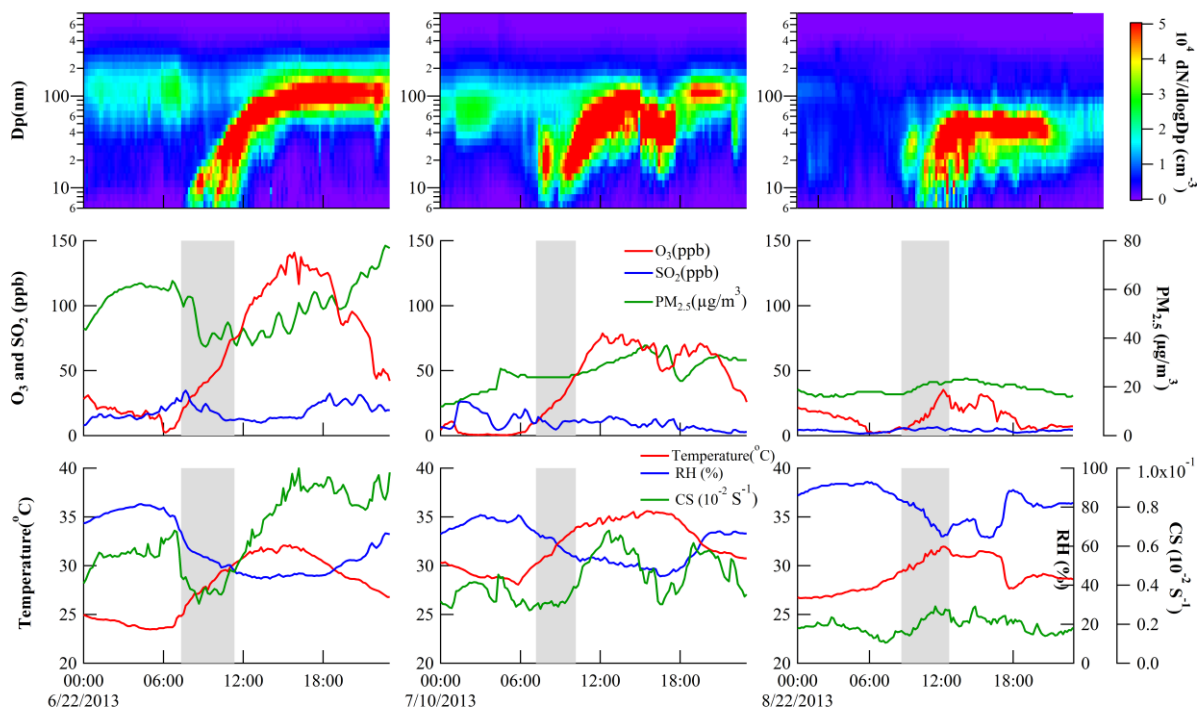


1

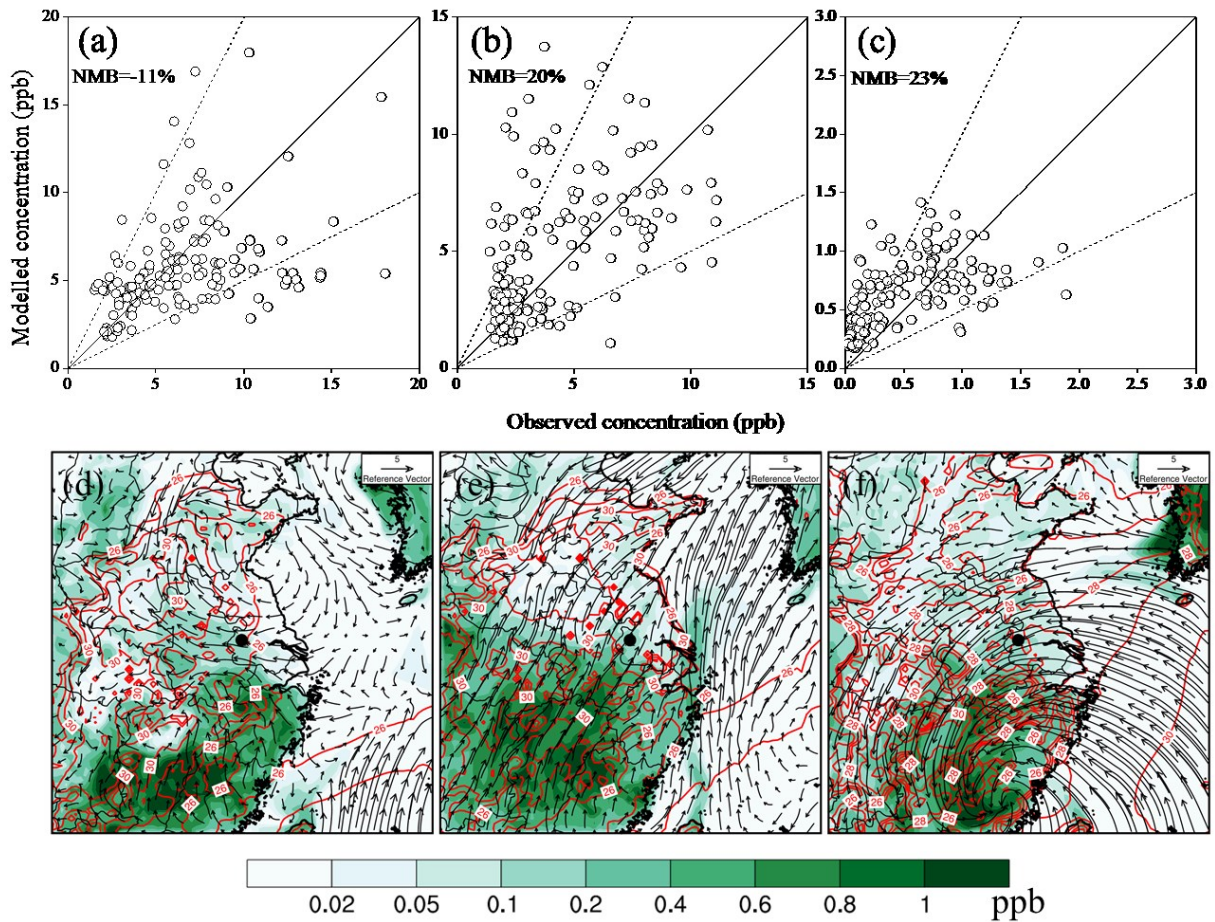
2 Figure 2. Retroplume (footprint residence time) showing transport pathways of air masses
 3 measured at the SORPES site for 22 June (a), 10 July (b) and 22 August(c). Spatial
 4 distributions of anthropogenic SO_2 (d), primary $\text{PM}_{2.5}$ (e) and biogenic monoterpene (f)
 5 emission rates.

6

7

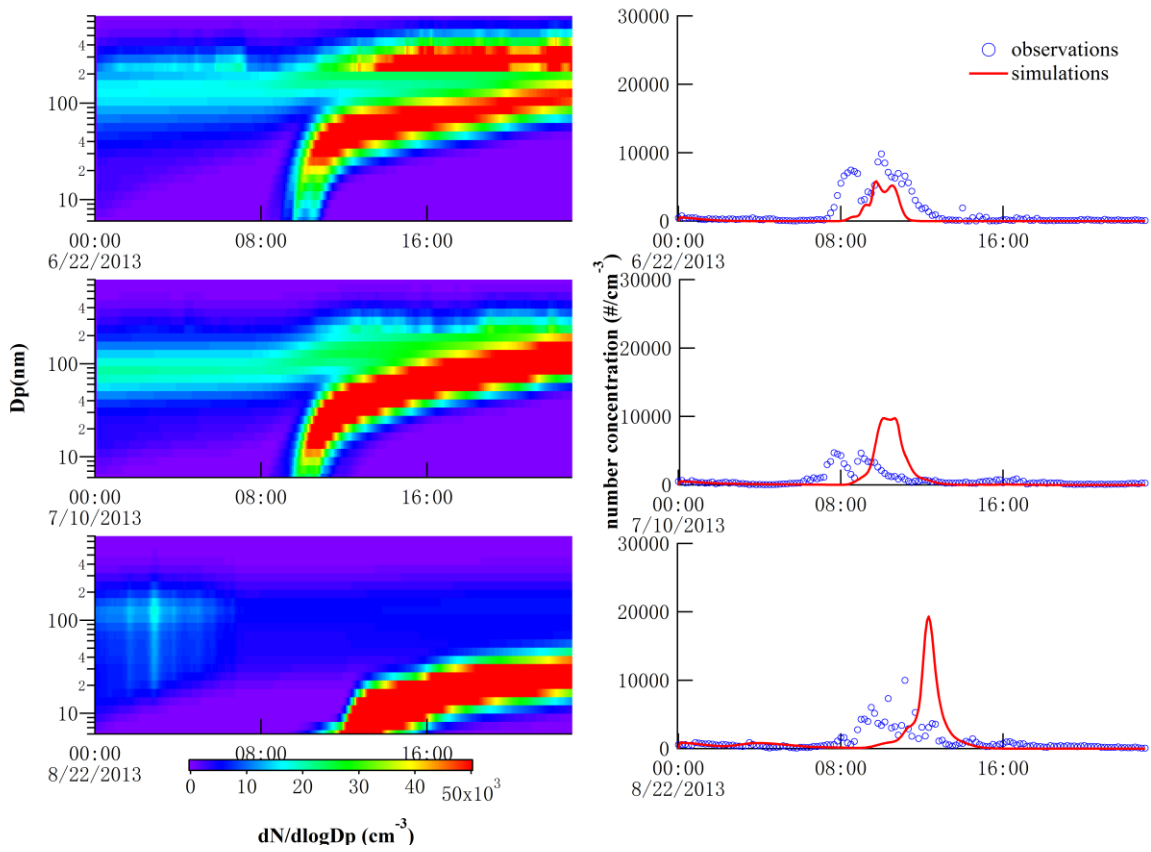


1
 2 Figure 3. Measured diurnal variations of particle size distributions (upper panel),
 3 concentrations of SO_2 , O_3 and $\text{PM}_{2.5}$ (middle panel), and meteorological conditions (bottom
 4 panel) during the three NPF days. Grey boxes show the time span of NPF events.

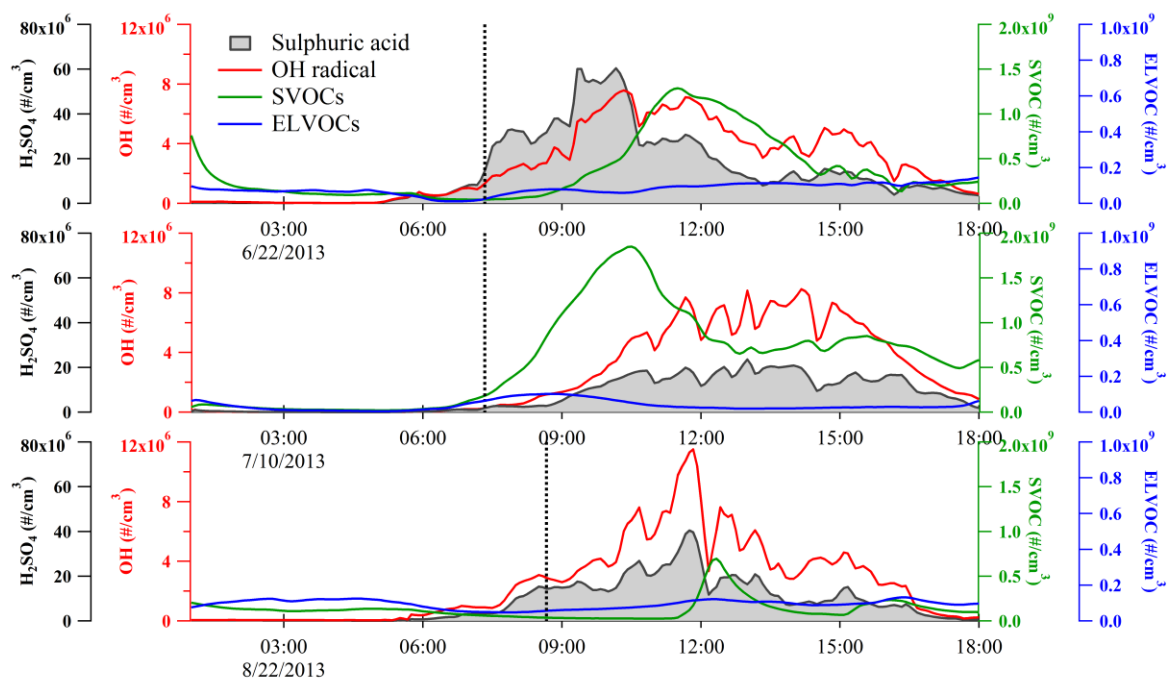


1
2
3
4
5
6
7
8

Figure 4. Scatter plots of observed and simulated alkene (a) aromatic (b) and isoprene (c) concentrations (NMB represents the normalized mean bias) in August 2014. The solid 1:1 lines and dashed 1:2 and 2:1 lines are shown for reference. Spatial distributions of terpene concentrations at 9:00 LT on 22 June (d), 10 July (e), and 22 August (f), 2013. 2-meter temperature are marked in red lines. The black dot marks the location of the SORPES station.

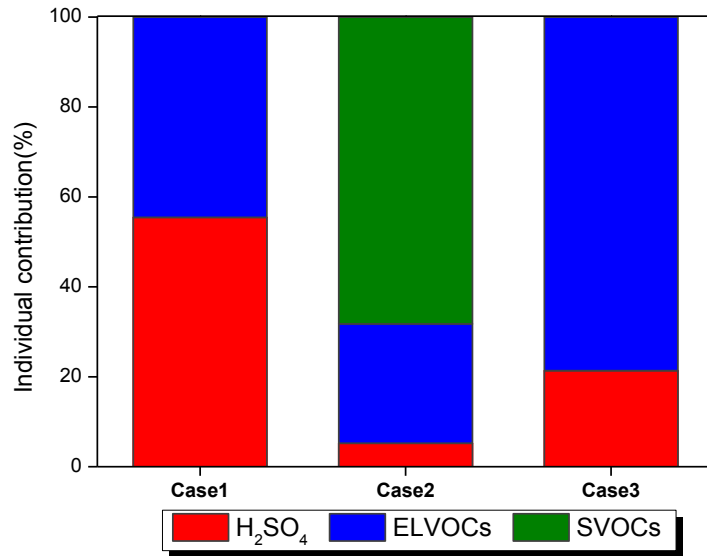


1
 2 Figure 5. Modelled pattern of particle size distributions (left panel) and number
 3 concentrations of particles ranging from 6 to 10 nm during these 3 NPF days (right panel).
 4
 5



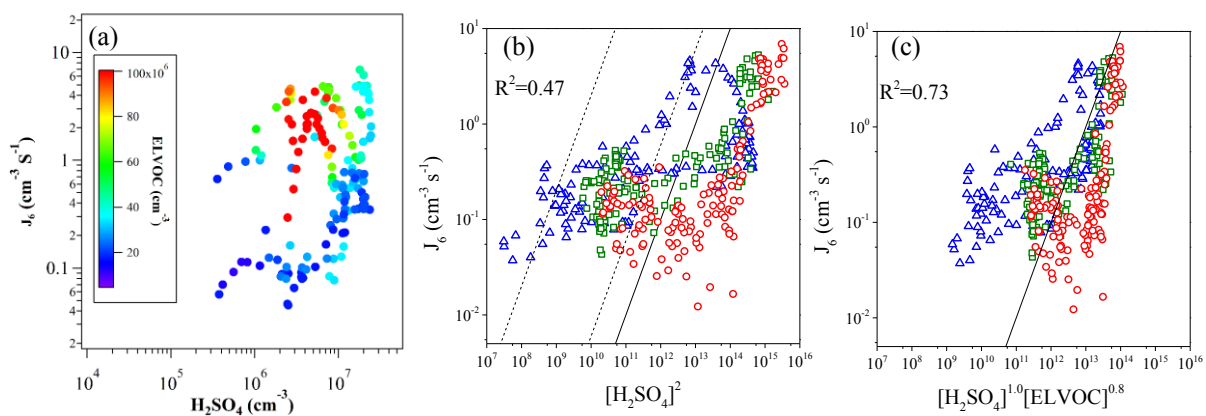
1
 2 Figure 6. Time series of several gas concentrations ($\# \text{ cm}^{-3}$) during the three selected NPF
 3 days. Sulphuric acid, OH radical, SVOCs and ELVOCs are marked in grey area, red, green
 4 and blue lines, respectively. Dashed lines show the onset time of NPF according to DMPS
 5 measurements for reference.

6



1
2
3
4
5

Figure 7. Contributions from three kinds of condensing vapours to growth of particle less than 10 nm during NPF events on 22 June (Case1), 10 July (Case2), and 22 August (Case3). Sulphuric acid, SVOCs and ELVOCs are marked in red, green and blue bars, respectively.



1
 2 Figure 8. Correlations of estimated new particle formation rates (J_6) from DMPS
 3 measurements with modelled gaseous sulphuric acid and ELVOC concentrations for event
 4 days between 06:00 and 16:00 (a). Scatter plots of new particle formation rate J_6 estimated
 5 from measurements with modelled sulphuric acid and ELVOC concentrations (b-c), in which
 6 red, blue and green markers refer to June 22, 10 July and 22 August, respectively. The square
 7 of correlation coefficients (R^2) are labelled in (b) and (c). Black solid lines denote $y=10^{-13}x$.
 8 Dashed lines show $y=2.2 \times 10^{-10}x$ (left) and $y=6.0 \times 10^{-13}x$ (right) for reference in (b).